Inclusive electroproduction from protons and deuterons

J. F. Martin, G. J. Feldman, G. Hanson, D. E. Lyon,* M. L. Perl, and T. P. Pun†
Stanford Linear Accelerator Center, Stanford University, Stanford, California 94305

C. Bolon, R. C. Lanza, D. Luckey, L. S. Osborne, and D. G. Roth‡
Laboratory for Nuclear Science, Massachusetts Institute of Technology, Cambridge, Massachusetts 02139

J. T. Dakin§
Department of Physics and Astronomy, University of Massachusetts, Amherst, Massachusetts 01002
(Received 14 August 1978)

We present results on the inclusive distributions of final-state hadrons created in deep-inelastic electron scattering from protons and deuterons. Data were taken from all portions of the kinematic range simultaneously in an apparatus which had equal detection efficiency for both charge signs. A subset of the produced hadrons were identified with a threshold-type Čerenkov counter. We find that the charge ratio h^+/h^- is a strong function of Q^2, x_F, and $p_T{}^2$, with little dependence on s. The ratio of production of h^- from deuterium to that from hydrogen as a function of ϕ is flat. The invariant cross section for each charge sign and each target exhibits the seagull effect (a correlation in $\langle p_T \rangle$ and $\langle x_F \rangle$). The value of $\langle p_T \rangle$ for data in the range $0.4 < x_F < 0.85$ increases slightly as Q^2 increases. The exponential dropoff in p_T for production of protons and kaons is similar to that for pions. The dropoff in x_F for production of pions shows a definite dependence on Q^2, but this effect is largely caused by the decay products of the exclusive ρ^0 final state. Finally, $f(x_F)$ for π^+, π^-, K^+, K^-, p, and $\bar{p}$ is presented for each target type.

I. INTRODUCTION

The method of high-energy deep-inelastic electron scattering has been combined with observation of hadrons produced in the forward direction in a very-high-statistics experiment performed at the Stanford Linear Accelerator Center (SLAC). This study is an improvement over a previous similar experiment[1] in that the quantity of data was 40 times larger and particle-identification capability was added.

The primary motivation for this study was a result[1] which indicated that the interaction of a virtual photon with a neutron (Fig. 1) produced a net positive charge in the mesons detected in the photon-fragmentation region. This was surprising, and was most easily explained via the quark model but the result was not compelling for two reasons. First, the experiment lacked particle-identification capability, so that production of either K^+ or p could have affected the final values, and second, the experiment lacked sufficient statistics.

The experiment reported here has succeeded in measuring the forward charge ratio of π^+ to π^- for neutrons[2]; furthermore, it proved capable of measuring in a new way some of the fundamental features of the substructure of the nucleon.[3] However, the purpose of this paper is to detail the experimental and analytic procedures employed, and to summarize the other results of the experiment for hydrogen and deuterium targets. Many of these results will be of value in comparing with other experiments which do not effect particle identification, or to theoretical calculations which do not distinguish particle types. The publications referred to above[2,3] covered the most important features of the π^+/π^- ratios; consequently, this paper will concentrate on h^+/h^- ratios and on the structure functions for all particle types. Data were also taken with targets of beryllium, carbon, copper, and tin; the primary results from that part of the experiment are reported in Ref. 4.

II. APPARATUS

Figure 2 shows a schematic drawing of the experiment. The beam of 20.5-GeV electrons measured 0.4 mm × 0.8 mm [full width at half maximum (FWHM)] at the target with an angular diver-

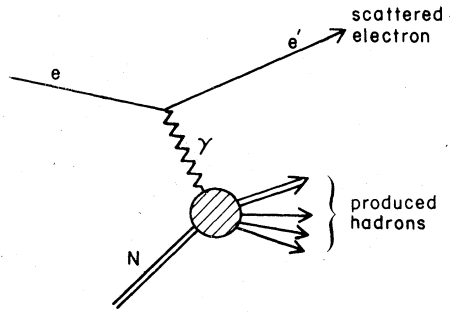

FIG. 1. Diagram representing inclusive electroproduction. In this experiment, N was either a neutron or a proton.

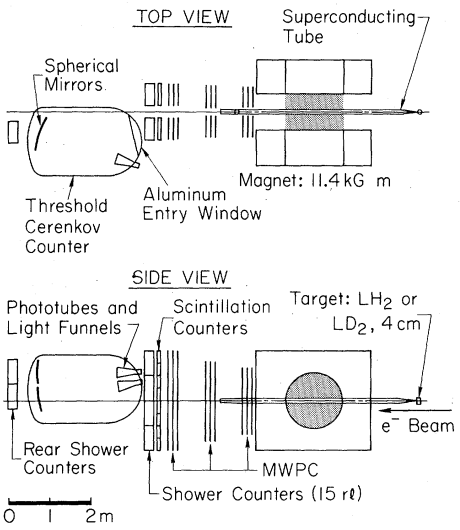

FIG. 2. Schematic description of the experimental apparatus.

gence of 0.20 mrad × 0.20 mrad (FWHM). The number of electrons in the beam averaged 3×10^5 per SLAC pulse, or 5×10^7 electrons per second. The integrated beam flux for the data in this paper is 5.3×10^{13} electrons on a hydrogen target (0.28 g/cm^2) and 4.6×10^{13} electrons on a deuterium target (0.64 g/cm^2).

The target cell was a 4-cm-diameter cylinder with its axis perpendicular to the beam. It was constructed of 64-μm-thick Kapton (a polyimide film), and except during target-empty runs, was filled with either liquid hydrogen or liquid deuterium.

The target was followed immediately by a large-aperture dipole magnet[1] and a superconducting transport tube which provided a totally field-free path for the beam emerging from the target. In this way, the main flux of the beam was excluded from the chambers and counters. This tube was very similar to that used in Ref. 1 and was one of the key factors allowing such high beam intensities.

The array of 18 multiwire proportional chambers (MWPC) started just downstream of the magnet and was arranged as three triplets on each side of the transport tube. Each triplet consisted of one chamber with wires strung horizontally, one chamber with wires at +30° to the horizontal, and one chamber with wires at −30° to the horizontal. The design of the chambers was conventional but very large, with an active area of 50 cm × 250 cm. The anode-to-anode spacing was 2 mm.

Immediately after the last triplets of MWPC was an array of 16 scintillation trigger counters, eight on each side of the beam tube. After corrections for the track position, the FWHM of the time-of-flight distribution was 2.8 ns. The apparatus was backed up by lead-scintillator sandwich shower counters[5] which served to identify scattered electrons for the trigger and off-line analysis. In one place, one of the shower counters was removed and a variable pressure threshold-type Čerenkov counter installed. It was pressurized with Freon 12 (CCl_2F_2) and had a thin (0.953 cm of aluminum) front window. Two spherical mirrors inside focused Čerenkov light onto two Amperex 58 DVP phototubes. This counter was backed up by two shower counters identical to the seven upstream. The fractional rms energy resolution of these counters was measured to be $0.024 + 0.29/\sqrt{E}$, E in GeV.

Finally, contoured lead blocks were placed around the transport tube and within the Čerenkov counter to provide additional shielding for the chamber and counter arrays. The design of all elements was controlled so that scattered electrons and produced hadrons could be detected down to 33 mrad (horizontally) from the incident beam direction.

The instantaneous beam intensity was monitored by a surface barrier detector[6] and the integrated beam flux was measured with a conventional quantameter.[7]

Two triggers were employed simultaneously, a "data" trigger and a "randoms" trigger. The data trigger consisted of at least one coincidence between a scintillation counter and a shower counter, in which the shower counter contained a pulse larger than that corresponding to a 3-GeV electron. This "single-arm" trigger was independent of whether hadrons entered the detector, and was therefore unbiased with regard to hadron detection. For each trigger a PDP-8 computer recorded which of the 11 520 wires fired, the time of flight of each fired scintillation counter and each Čerenkov phototube, and the pulse height in each fired shower counter and each Čerenkov phototube. The integrated beam flux, magnetic field, Čerenkov pressure, and target type were also recorded. The randoms trigger was enabled every thirtieth beam pulse during the pulse. It yielded events in which the effects of chance coincidences in the chambers and counters could be studied.

The Čerenkov counter was operated at four different pressures 0.51, 1.56, 2.86, and 6.80 atm (7.5, 23.0, 42.0, and 100 psia, respectively). At each pressure roughly equal amounts of data were taken for each magnet polarity. This yielded eight blocks of data for each target type. We collected 8×10^6 triggers from deuterium and 4×10^6 triggers from hydrogen.

III. DEFINITION OF VARIABLES

The kinematic variables which depend only on the scattering of the electron are Q^2, the absolute value of the transverse momentum squared of the virtual photon, ν, the energy of the virtual photon, and s, the energy squared of the virtual-photon–nucleon system. Then we define the scaling variable

$$x = Q^2/2M\nu, \quad \text{where } M = \text{proton mass}. \tag{1}$$

A similar variable

$$x' = Q^2/(Q^2 + s) \tag{2}$$

is also used in one of the graphs in order to compare to previous results.

The kinematic variables in the photon-proton center of mass relevant to the single-particle inclusive cross section for the produced hadrons are $x_F = p_l/p_{\max}$ with $p_{\max} = \sqrt{s}/2$, p_T^2 = the square of the momentum transverse to the virtual-photon direction, and ϕ = the azimuthal angle of the hadron about the direction of the virtual photon. ϕ is defined such that it is zero when the scattered electron-hadron opening angle is smallest.

There are therefore five variables for each charge sign of the hadrons. Note that we have chosen the simplest definition of $p_{\max}$; it is independent of particle type. Instead of x_F, the variable $z = p_{\text{lab}}/\nu$ is often used. Table I shows how closely z and x_F correspond for pions at a typical Q^2 and s for two values of p_T^2.

With the appropriate kinematic factors folded in, we then define (as in Ref. 1) the cross sections which are frequently used to describe leptoproduction results.

The invariant differential cross section equals

$$\frac{E}{\sigma_{\text{tot}}}\frac{d^3\sigma}{dp^3} = \frac{1}{\sigma_{\text{tot}}}\frac{2E}{p_{\max}}\frac{d\sigma}{dp_T^2 d\phi\, dx_F}, \tag{3}$$

where E and p refer to the hadron in the center of mass of the photon-nucleon system and σ_{tot} is the electron scattering cross section. The structure function in x_F is $f(x_F)$ and equals

$$\frac{1}{2\pi}\frac{2}{\sigma_{\text{tot}}}\int \frac{E}{p_{\max}}\frac{d\sigma}{dp_T^2 d\phi\, dx_F}\, dp_T^2\, d\phi\,. \tag{4}$$

The probability distribution in x_F is dN/dx_F and equals

$$\frac{1}{\sigma_{\text{tot}}}\int \frac{d\sigma}{dp_T^2 d\phi\, dx_F}\, dp_T^2\, d\phi\,. \tag{5}$$

$f(x_F)$ and $(x_F/\pi)dN/dx_F$ are often used interchangeably but in fact are related in only an approximate way. Table II shows the ratio of these two functions as calculated for the data reported here.

TABLE I. Correspondence of x_F and z at two values of p_T^2 in $(\text{GeV}/c)^2$ for $Q^2 = 1.0\ (\text{GeV}/c)^2$ and $s = 21\ \text{GeV}^2$.

x_F	z for $p_T^2 = 0.0$	z for $p_T^2 = 0.25$
0.10	0.110	0.181
0.20	0.205	0.257
0.30	0.303	0.342
0.40	0.402	0.433
0.50	0.502	0.527
0.60	0.601	0.623
0.70	0.701	0.719
0.80	0.800	0.817
0.90	0.900	0.915

TABLE II. Ratio of $x_F dN/dx_F$ to $\pi f(x_F)$ at typical Q^2 and s.

$\langle x_F \rangle$	Ratio
0.05	0.27
0.15	0.65
0.25	0.80
0.35	0.87
0.45	0.91
0.55	0.93
0.72	0.95
0.92	0.97

IV. DATA REDUCTION AND ANALYSIS

The three sense wire angles in the MWPC measured three coordinates, labeled x, u, and v. The fired wires were first combined into lines in x, u, and v separately; these lines were then combined to make tracks in space. The reconstruction algorithm allowed one chamber in each group of nine to be missing; that is, if two or more were missing, no track was declared. Per event, the average number of tracks was 1.1 and the average number of hits per chamber was 5. Most of the hits were caused by materialization of low-energy photons (down to 1 MeV) from the process $e^- + e^- \to e^- + e^- + \gamma$. This background limited the beam intensity at which we could take data.

The requirements for each track were the following:

(a) It must fit a straight line in space with a χ^2 per degree of freedom of less than 4.

(b) Its horizontal projection must extrapolate to within ± 4 cm of the target.

(c) The counters it projected to must have fired.

The tracks meeting these requirements were then momentum analyzed. The magnet was of an open design and therefore the field was nonuniform. Nevertheless, by taking advantage of the symmetry of the field a simple computer routine

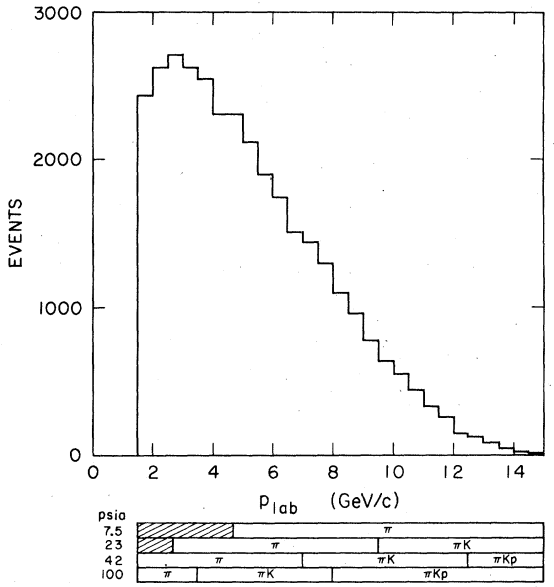

FIG. 3. Laboratory momentum spectrum for all hadrons (h^+ and h^-) entering the Čerenkov-counter fiducial volume. The data are summed over both targets. Using the same abscissa scale, the bar graph underneath shows the momentum bands within which π, K, and p are energetic enough to be detected.

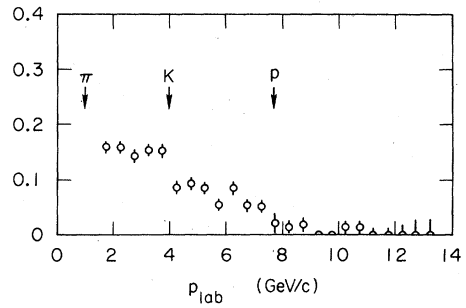

FIG. 4. Ratio of unfired tracks to all tracks for all 100-psia data. The arrows indicate the Cerenkov-counter threshold for each particle type.

was found which did not require tracking the particle step by step back through the magnetic field. Instead, first-order values of the momentum and the angles of emergence from the target were found, and these were modified by an empirical correction matrix based on the point of emergence from the magnet. This routine was accurate to better than 0.3% in momentum and angle, matching the inherent accuracy of the chambers.

Finally, the scattered electrons were identified by requiring a shower counter pulse consistent with the track's momentum. The total number of detected electrons was 2×10^6, and the number of these with one or more produced hadrons in a forward solid angle of 60 msr was 5×10^5.

Tracks entering the fiducial region of the Čerenkov counter were subjected to further restrictions in time of flight and pulse height to determine if that counter was fired. Figure 3 shows the raw momentum distribution of hadrons entering the Čerenkov counter and the bands of its sensitivity to various particle types.

The variables described above were each divided into several bins; for each charge sign this yielded a total of 21 168 bins in a five-dimensional array. Within each there were only small variations in the detector efficiency. Each scattered electron-produced hadron combination has been treated as a separate "double-arm" event in our analysis. However, it does not effect any of the conclusions in this paper, if for example, the scattered electron was combined with only the most energetic of the detected hadrons.

Five classes of events were accumulated into these bins for each charge sign and each target:

Class 1: all double-arm events.

Class 2: the subset of class 1 entering the Čerenkov counter and falling within pion-only momentum bands $\equiv n_2$.

Class 3: the subset of class 2 which fired that counter $\equiv n_3$.

Class 4: the subset of class 1 entering the counter and falling within (pion or kaon)-only bands $\equiv n_4$.

Class 5: the subset of class 4 which did not fire the Čerenkov counter $\equiv n_5$.

Differential cross sections for class 1 ($=\sigma_h$) were calculated by applying the systematic corrections to the data bin by bin, and dividing by the number of scattered electrons in the appropriate (Q^2, s) range. Then, for the individual particle types, the production cross sections were in principle just

$$\sigma_\pi = \frac{n_3}{n_2}\sigma_h , \tag{6}$$

$$\sigma_p = \frac{n_5}{n_4}\sigma_h , \tag{7}$$

$$\sigma_K = \sigma_h - \sigma_\pi - \sigma_p . \tag{8}$$

In practice, additional corrections were made at this stage (see Sec. V).

TABLE III. Decay-loss correction factor for kaons.

x_F	Correction
0.25	1.35±0.03
0.35	1.27±0.03
0.45	1.20±0.02
0.55	1.16±0.02
0.72	1.12±0.01
0.92	1.10±0.01

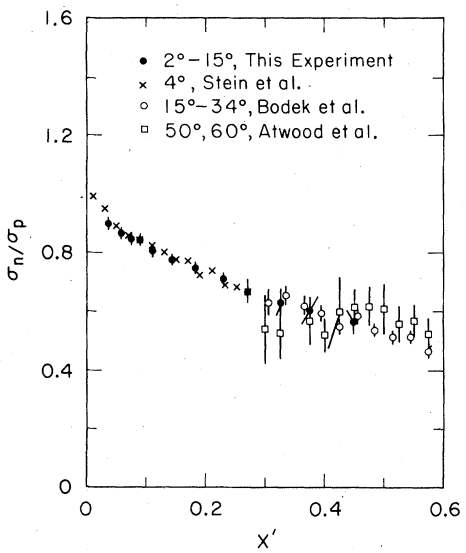

FIG. 5. Comparison of σ_n/σ_p with three other experiments. The data labeled Stein *et al.* are from Ref. 10, Bodek *et al.* are from Ref. 11, and Atwood *et al.* are from Ref. 12.

V. SYSTEMATICS

Except where noted below, all errors shown in this paper are a combination in quadrature of statistical and point-to-point systematic errors. Not shown is an additional uncertainty of ±10% in all values representing absolute invariant cross sections.

Inasmuch as the contamination of deuterium in the liquid hydrogen target was less than 0.2% and of hydrogen in the liquid deuterium target was less than 0.3%, no corrections for target contamination have been made.

The fractional detector resolution was $0.2p\%$ in p (p equals the laboratory momentum in GeV/c), 0.003 rad in θ_y, and 0.001 rad in θ_x. This was checked by comparing the missing-mass distribution for observed ρ^0 events in the data versus a Monte Carlo simulation of exclusive ρ^0. The effect of this resolution on the kinematic variables for the hadron used in this paper was calculated to be $dx_F = 0.008 + 0.04\ x_F$, $dp_T{}^2 = 0.009 + 0.03\ p_T{}^2$ (in GeV/c^2), and $d\phi = 0.05$ rad. The resulting error in the exponential slope in the distributions in $p_T{}^2$ and x_F is less than +0.02 and was therefore ignored.

We now describe the systematic corrections made in the order in which they were applied.

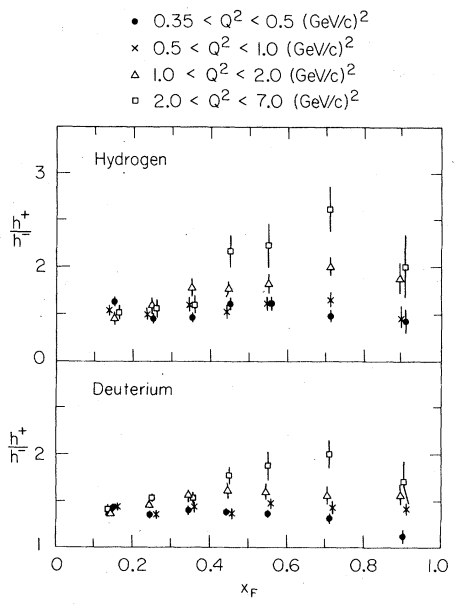

FIG. 6. Ratio of h^+ to h^- as a function of x_F and Q^2.

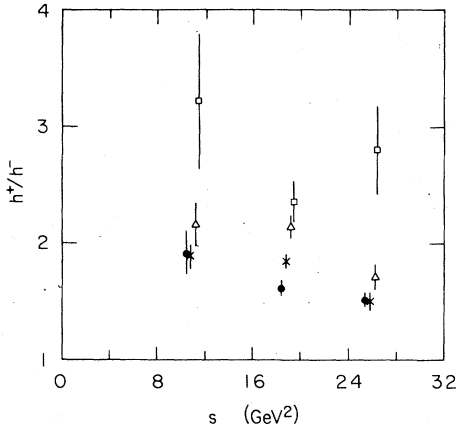

FIG. 7. Ratio of h^+ to h^- as a function of s and Q^2 for production from hydrogen. The symbols are as shown in Fig. 6. The data have been integrated over x_F from 0.4 and 0.85.

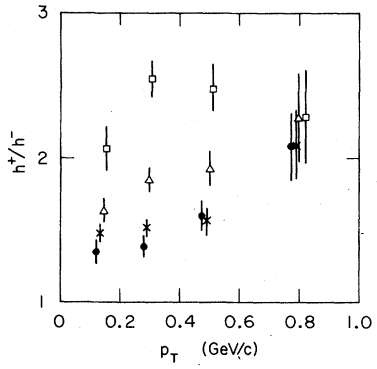

FIG. 8. Ratio of h^+ to h^- as a function of p_T and Q^2 for production from hydrogen. The symbols are as shown in Fig. 6. The data have been integrated over x_F from 0.4 and 0.85.

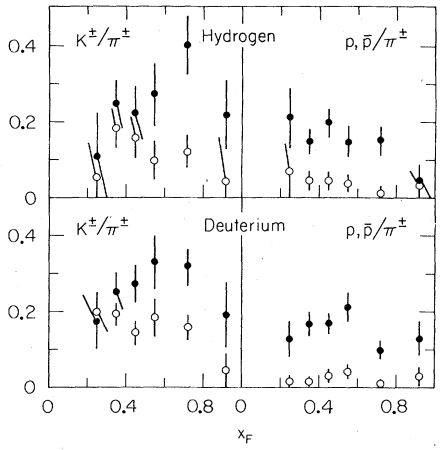

FIG. 9. Ratio of $K^{\pm}/\pi^{\pm}$ and $p, \bar{p}/\pi^{\pm}$ for data integrated from 0.5 to 7.0 $(\mathrm{GeV}/c)^2$ in Q^2 (see Table X). The filled symbols are for positives and the open symbols for negatives.

A. Random track backgrounds

In addition to the good tracks, there were spurious tracks resulting from the large number of converted photons and from low-energy beam-pipe associated particles. Although these were largely eliminated using the restrictions in Sec. IV above, a small fraction remained, amounting to 0.3% of all real hadrons. A special data file was constructed in which each event was a combination of a real electron and a randomly chosen hadron from the randoms-triggered data. These data were then subtracted from the normal data using the number of scattered electrons for normalization. We estimate the systematic error introduced by this procedure into any of the results presented here to be less than 0.10%.

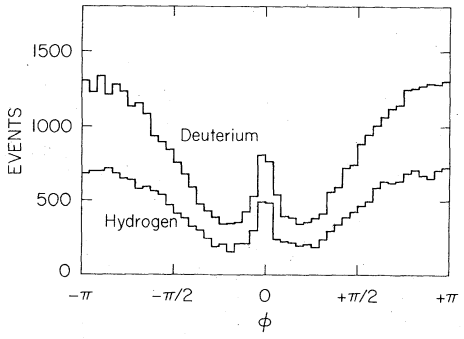

FIG. 10. Uncorrected ϕ spectrum for h^- production from each target. The data have been integrated over Q^2 from 0.35 to 1.0 $(\mathrm{GeV}/c)^2$ and over x_F from 0.4 to 0.85.

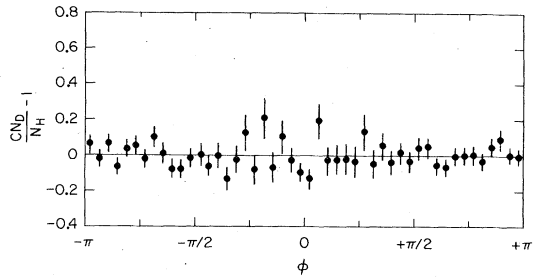

FIG. 11. Ratio of the h^- production from deuterium to that from hydrogen minus unity. The data are those shown in Fig. 10 where deuterium data have been multiplied by an arbitrary normalization constant. This ratio is designed to reveal any differences between neutrons and protons in production versus ϕ.

B. Target-empty backgrounds

At 16 times during the runs, target-empty data were logged. These data were analyzed exactly like the target full data, and then subtracted from them using the number of incident electrons for normalization. The correction averaged about 5% for deuterium and about 10% for hydrogen. Enough data were taken so that the additional statistical error introduced by the subtraction of this data was less than 10% of the statistical error inherent in each target-full sample.

C. Track efficiency

One of the goals of this experiment was to run at the highest possible intensity. Studies were therefore made at the beginning in which track efficiency was studied as a function of incident beam intensity. The track efficiency was quite flat up to and including 5×10^5 electrons per pulse. Beyond that, it began to drop off; i.e., so many hits were being recorded that the chamber dead time was limiting genuine track information. Hence, we ran at 3×10^5 for hydrogen which turned out to be quite conservative. Naturally, the conservative value was a function of the number

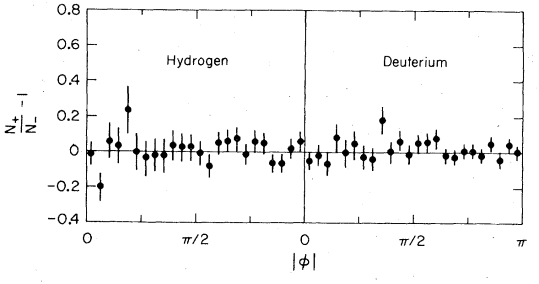

FIG. 12. N^+ is the number of h^- events from Fig. 10 in a particular $+|\phi|$ bin, and N^- is that at $-|\phi|$. This ratio is designed to reveal any asymmetry about $\phi = 0$.

of g/cm^2 in the target and was 1.4×10^5 for the deuterium runs.

The final track efficiency was a combination of chamber and counter dead time and chamber efficiency, and was measured to be 95% and uniform throughout the fiducial volume to ±1%. This track efficiency was also measured as a function of each kinematic variable and found to be flat to within ±1%.[8]

D. Misidentification of e^- and h^-

A small fraction of the time the scattered electron e^- and one of the produced negative hadrons h^- would enter the same shower counter. In a subset of these events the shower produced would have a pulse height which (owing to the relatively coarse energy resolution) would imply a momentum value closer to the momentum of the h^- than to that of the e^-.

A second source of error was that in some cases in which the scattered e^- was not detected, an h^- interaction in the shower counters (in an h^-h^+ or h^-h^- event) would yield a pulse height near that of an e^-. A simple calculation in which h^+ were used allowed us to make a momentum-dependent correction (which varied from 0 to 6%) to the data for these effects.

E. Geometric efficiency

No estimate of the geometric efficiency was needed to calculate particle-type ratios since the apparatus response was (charge- and angle-) symmetric to within 1%. However, to calculate invariant cross sections, it was necessary to construct a Monte Carlo simulation of the detector. This program generated events with the same physical parameters as the data, and binned both generated and detected hadrons with the same binning architecture employed with the data. Roughly 50 times the number of data events were generated, and for each an h^+ and h^- were passed through a detector simulator. In this way, model-dependent effects were largely eliminated. Furthermore, in constructing the cross sections, data from regions in which the calculated detector efficiency was less than 1% were eliminated to avoid systematic errors resulting from large geometrical corrections. This lower bound on the efficiency was then varied, and the cross sections studied for the effect this had. Some shifting of the results as a function of the lower bound could be seen, but it was generally less than 2%, and always less than 5%. Hence, we have added a 5% point-to-point error to all the cross-section results.

F. Čerenkov-counter effects

Figure 4 shows the ratio of (nonfiring tracks) to (all tracks) within the fiducial volume of the Čerenkov counter as a function of momentum. The data in Fig. 4 are for 6.80 atm only, and above 7.5 GeV/c the ratio should be 0.0 if the counter were 100% efficient. Thus we have a measure of the counter's efficiency 99.0 ± 0.3%. A certain fraction of the tracks entering the Čerenkov counter which should not have fired it came in coincidence with background radiation from the beam pipe. This fraction was a function of the counter pressure and was measured using those events which did not have a track near the Čerenkov counter. We find the fraction to be 0.070 ± 0.002 at 0.51 atm, 0.119 ± 0.003 at 1.56 atm, 0.146 ± 0.005 at 2.86 atm, and 0.236 ± 0.010 at 6.80 atm. An independent check was made by comparing the π/h ratios from different pressures at the same momentum; this agreed with results based on these values.

G. π,K decay in flight

The decay of pions and kaons in flight affected the final K/π ratios as well as the absolute cross

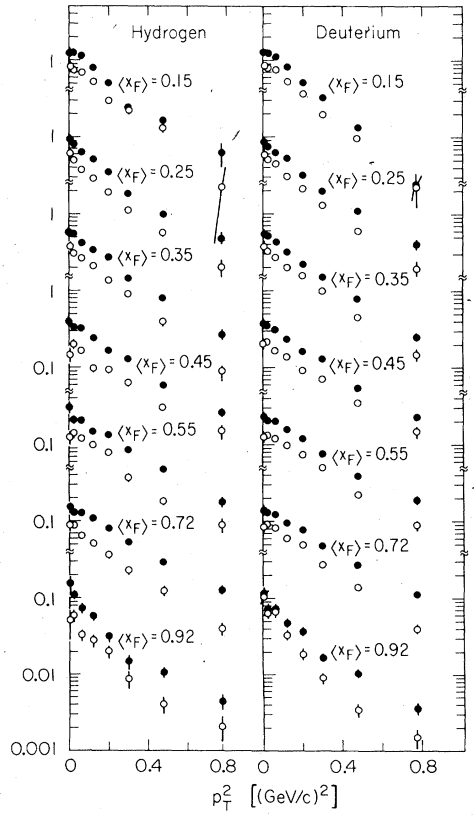

FIG. 13. Invariant cross section (see text) for h^+ (filled symbols) and h^- (open symbols) as a function of p_T^2 for seven x_F bands. These data have been integrated over Q^2 from 1.0 to 5.0 (GeV/c)^2.

TABLE IV. Average p_T in GeV/c versus Q^2 and x_F for $15 < s < 31$ GeV^2.

Q^2 [(GeV/c)^2]	x_F	Hydrogen h^-	Hydrogen h^+	Deuterium h^-	Deuterium h^+
0.42	0.05	0.317 ± 0.022	0.337 ± 0.022	0.314 ± 0.015	0.336 ± 0.015
0.42	0.15	0.310 ± 0.018	0.341 ± 0.013	0.320 ± 0.015	0.337 ± 0.015
0.42	0.25	0.389 ± 0.022	0.380 ± 0.015	0.382 ± 0.015	0.396 ± 0.013
0.42	0.35	0.413 ± 0.027	0.423 ± 0.018	0.399 ± 0.013	0.410 ± 0.012
0.42	0.45	0.414 ± 0.022	0.464 ± 0.029	0.415 ± 0.015	0.444 ± 0.015
0.42	0.55	0.430 ± 0.030	0.460 ± 0.022	0.422 ± 0.024	0.452 ± 0.017
0.42	0.72	0.419 ± 0.019	0.446 ± 0.017	0.413 ± 0.013	0.432 ± 0.011
0.42	0.92	0.361 ± 0.036	0.410 ± 0.030	0.351 ± 0.022	0.419 ± 0.024
0.72	0.05	0.323 ± 0.020	0.319 ± 0.014	0.319 ± 0.013	0.319 ± 0.011
0.72	0.15	0.338 ± 0.015	0.321 ± 0.015	0.325 ± 0.015	0.322 ± 0.012
0.72	0.25	0.378 ± 0.015	0.387 ± 0.014	0.378 ± 0.014	0.380 ± 0.015
0.72	0.35	0.432 ± 0.022	0.425 ± 0.025	0.418 ± 0.014	0.417 ± 0.011
0.72	0.45	0.429 ± 0.022	0.423 ± 0.015	0.431 ± 0.016	0.428 ± 0.012
0.72	0.55	0.427 ± 0.019	0.481 ± 0.027	0.419 ± 0.014	0.464 ± 0.015
0.72	0.72	0.420 ± 0.018	0.476 ± 0.016	0.433 ± 0.013	0.462 ± 0.011
0.72	0.92	0.337 ± 0.022	0.431 ± 0.026	0.366 ± 0.018	0.384 ± 0.016
1.4	0.05	0.286 ± 0.029	0.321 ± 0.021	0.305 ± 0.020	0.312 ± 0.015
1.4	0.15	0.330 ± 0.020	0.324 ± 0.015	0.315 ± 0.015	0.315 ± 0.015
1.4	0.25	0.364 ± 0.020	0.379 ± 0.018	0.367 ± 0.014	0.382 ± 0.012
1.4	0.35	0.403 ± 0.026	0.411 ± 0.020	0.400 ± 0.017	0.429 ± 0.018
1.4	0.45	0.459 ± 0.038	0.465 ± 0.028	0.445 ± 0.023	0.449 ± 0.019
1.4	0.55	0.444 ± 0.039	0.527 ± 0.052	0.465 ± 0.031	0.476 ± 0.028
1.4	0.72	0.428 ± 0.026	0.485 ± 0.022	0.440 ± 0.018	0.480 ± 0.016
1.4	0.92	0.430 ± 0.053	0.429 ± 0.034	0.363 ± 0.028	0.443 ± 0.031
3.1	0.05	0.333 ± 0.085	0.290 ± 0.040	0.278 ± 0.045	0.296 ± 0.029
3.1	0.15	0.298 ± 0.023	0.296 ± 0.020	0.279 ± 0.020	0.296 ± 0.020
3.1	0.25	0.332 ± 0.036	0.368 ± 0.028	0.368 ± 0.029	0.367 ± 0.021
3.1	0.35	0.338 ± 0.018	0.398 ± 0.041	0.389 ± 0.031	0.418 ± 0.027
3.1	0.45	0.390 ± 0.048	0.441 ± 0.051	0.509 ± 0.063	0.450 ± 0.037
3.1	0.55	0.472 ± 0.072	0.481 ± 0.055	0.465 ± 0.050	0.486 ± 0.044
3.1	0.72	0.474 ± 0.060	0.528 ± 0.078	0.447 ± 0.043	0.507 ± 0.047
3.1	0.92	0.356 ± 0.085	0.542 ± 0.135	0.350 ± 0.047	0.444 ± 0.058

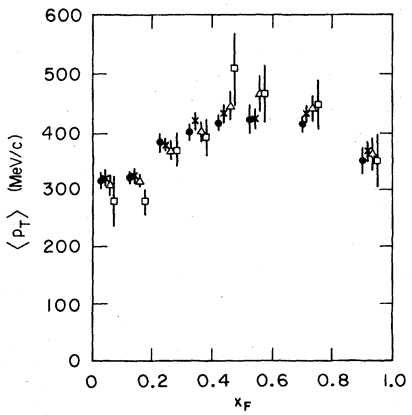

FIG. 14. Average p_T for h^- in MeV/c as a function of x_F for four Q^2 bands. The symbols are shown in Fig. 6.

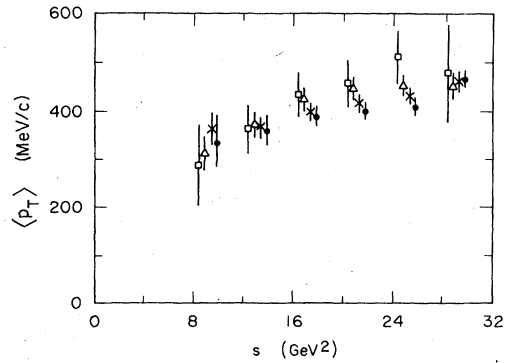

FIG. 15. Average p_T for h^- in MeV/c as a function of s for four Q^2 bands. The symbols are as shown in Fig. 6. The data have been integrated over x_F from 0.4 to 0.85.

TABLE V. Average p_T in GeV/c versus Q^2 and s for $0.4 < x_F < 0.85$.

s (GeV^2)	Q^2 [(GeV/c)^2]	Hydrogen h^-	Hydrogen h^+	Deuterium h^-	Deuterium h^+
9	0.42	0.311 ± 0.079	0.375 ± 0.084	0.332 ± 0.053	0.350 ± 0.056
13	0.42	0.354 ± 0.042	0.384 ± 0.037	0.359 ± 0.030	0.384 ± 0.028
17	0.42	0.391 ± 0.032	0.418 ± 0.026	0.387 ± 0.021	0.416 ± 0.020
21	0.42	0.401 ± 0.026	0.434 ± 0.022	0.399 ± 0.016	0.428 ± 0.016
25	0.42	0.439 ± 0.022	0.450 ± 0.018	0.410 ± 0.015	0.453 ± 0.014
29	0.42	0.452 ± 0.026	0.508 ± 0.023	0.467 ± 0.018	0.476 ± 0.016
9	0.72	0.376 ± 0.039	0.351 ± 0.027	0.366 ± 0.028	0.392 ± 0.024
13	0.72	0.379 ± 0.027	0.407 ± 0.022	0.368 ± 0.018	0.403 ± 0.016
17	0.72	0.382 ± 0.021	0.437 ± 0.017	0.398 ± 0.015	0.430 ± 0.014
21	0.72	0.421 ± 0.019	0.453 ± 0.017	0.416 ± 0.013	0.451 ± 0.012
25	0.72	0.441 ± 0.018	0.450 ± 0.015	0.432 ± 0.012	0.443 ± 0.010
29	0.72	0.455 ± 0.021	0.464 ± 0.017	0.462 ± 0.015	0.459 ± 0.012
9	1.4	0.331 ± 0.054	0.325 ± 0.029	0.314 ± 0.035	0.296 ± 0.022
13	1.4	0.352 ± 0.031	0.380 ± 0.024	0.373 ± 0.025	0.367 ± 0.017
17	1.4	0.409 ± 0.035	0.457 ± 0.028	0.426 ± 0.022	0.453 ± 0.021
21	1.4	0.456 ± 0.038	0.461 ± 0.024	0.447 ± 0.022	0.452 ± 0.016
25	1.4	0.457 ± 0.029	0.508 ± 0.027	0.454 ± 0.019	0.468 ± 0.017
29	1.4	0.451 ± 0.038	0.478 ± 0.029	0.452 ± 0.026	0.480 ± 0.021
9	3.1	0.256 ± 0.074	0.251 ± 0.049	0.287 ± 0.086	0.267 ± 0.043
13	3.1	0.340 ± 0.060	0.358 ± 0.037	0.367 ± 0.050	0.385 ± 0.032
17	3.1	0.396 ± 0.056	0.433 ± 0.039	0.434 ± 0.045	0.459 ± 0.034
21	3.1	0.460 ± 0.050	0.465 ± 0.046	0.458 ± 0.047	0.467 ± 0.031
25	3.1	0.499 ± 0.082	0.496 ± 0.043	0.517 ± 0.055	0.478 ± 0.034
29	3.1	0.463 ± 0.125	0.517 ± 0.096	0.483 ± 0.102	0.494 ± 0.075

sections for π only and K only. We used a Monte Carlo simulation of decay in which the following possibilities were included: (a) None of the decay products were accepted as good tracks; (b) a decay product might be accepted as good and, moreover, fire the Čerenkov counter; and (c) A decay product might be accepted as a good track but miss the Čerenkov counter. A decay-loss factor was calculated as a function of the kinematic variables and applied to both the π and K data after invariant cross sections were found. For pions this was a small effect, always less than 3%. Table III shows the size of this correction factor for kaons as a function of x_F for events integrated over $0.5 < Q^2 < 7.0$ (GeV/c)^2, $15 < s < 31$ GeV^2, and $0.0 < p_T{}^2 < 0.64$ (GeV/c)^2.

H. Neutron-target cross sections

Although it is beyond the scope of this study to measure the deep-inelastic electron scattering cross section, we can measure σ_n/σ_p. This serves as an independent check of the subtraction of hydrogen from deuterium employed to get the results in Refs. 2 and 3. The cross section for neutrons was extracted in the conventional way: For each x' bin

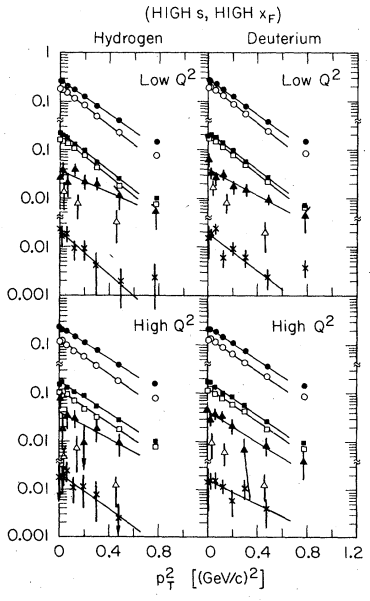

FIG. 16. Invariant cross section for each particle type. Filled symbols refer to +, open symbols to −. Circles correspond to all hadrons, squares to pions, triangles to kaons, and crosses to protons. Solid lines represent the fits described in Table VI.

TABLE VI. b [in $(\mathrm{GeV}/c)^{-2}$] from fit to $e^{-bp_T^2}$ for data in Fig. 16.

	Hydrogen		Deuterium	
	$0.35<Q^2<1.0$ $(\mathrm{GeV}/c)^2$	$1.0<Q^2<5.0$ $(\mathrm{GeV}/c)^2$	$0.35<Q^2<1.0$ $(\mathrm{GeV}/c)^2$	$1.0<Q^2<5.0$ $(\mathrm{GeV}/c)^2$
h^+	4.11 ± 0.05	3.76 ± 0.08	4.29 ± 0.07	3.89 ± 0.05
h^-	4.57 ± 0.10	4.12 ± 0.10	4.63 ± 0.11	3.99 ± 0.10
π^+	4.61 ± 0.15	3.77 ± 0.24	4.46 ± 0.17	4.02 ± 0.17
π^-	4.67 ± 0.25	3.93 ± 0.13	4.56 ± 0.12	3.95 ± 0.19
K^+	2.7 ± 0.75	3.1 ± 1.9	3.1 ± 0.8	3.69 ± 0.74
p	5.1 ± 1.5	4.4 ± 0.7	4.5 ± 1.4	3.0 ± 0.7

$$\sigma_n = f_1\sigma_d - \sigma_p, \quad f_1 = 1.02 \tag{9}$$

where σ_d and σ_p are the electron scattering cross sections for deuterons and protons, respectively, and 1.02 expresses the correction necessary to account for Fermi motion in the deuteron.[9]

Figure 5 shows the resulting value of σ_n/σ_p as a function of x' up to x' of 0.6, comparing it to previous results in that region. Our points agree well with experiments which took data at comparable scattering angles.

I. Elastic ρ^0 contribution

At low Q^2 the virtual-photon–nucleon interaction produces a final state of ρ^0 and nucleon. This is a process with a rather small amount of momentum transferred to the nucleon; in x_F terms it corresponds to x_F (as calculated for the $\pi^+\pi^-$ pair) of near 1.0. In the context of many models, such as vector dominance, this final state is analogous to that from elastic scattering and is not generally regarded as inclusive production. Therefore, it must be subtracted from any inclusive data in order to get inclusive cross sections. In this experiment often only the π^+ or π^- from such a decay was detected, making it impossible to know which events resulted from this exclusive ρ^0 production.

Consequently, where noted below, we have made a Q^2-dependent correction to the $f(x_F)$ values. The estimated ρ^0 contribution is shown graphically in Fig. 19 for the lowest Q^2 range 0.35 to 0.5 $(\mathrm{GeV}/c)^2$. The procedure used was to calculate the expected shape of the exclusive ρ^0 contribution to the data bin by bin with a Monte Carlo simulation routine and normalize this contribution by using the observed number of exlusive ρ^0's. The resulting correction was thus relatively insensitive to the detection efficiency and accurate to ±7%.

VI. SUMMARY OF RESULTS

Unless otherwise stated, the results presented below have been integrated over some range in the

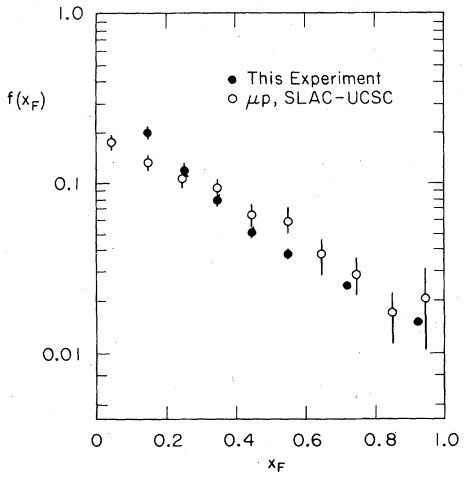

FIG. 17. Comparison of two measurements of the structure function for producing h^- from hydrogen. The filled circles correspond to the kinematic range 0.5 to 5.0 $(\mathrm{GeV}/c)^2$ in Q^2 and 11 to 23 GeV^2 in s. The open circles are from Ref. 15 and correspond to 0.5 to 4.5 $(\mathrm{GeV}/c)^2$ in Q^2 and 12 to 22 GeV^2 in s.

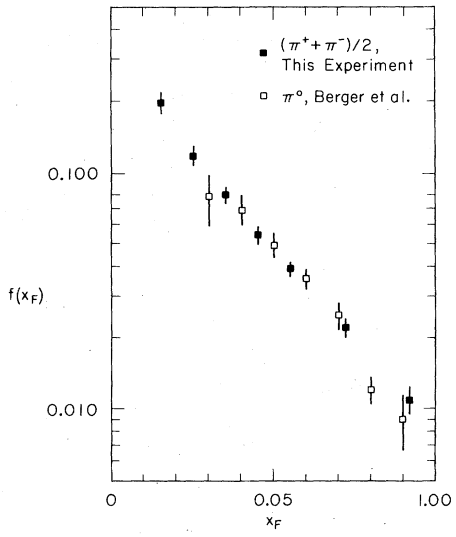

FIG. 18. Comparison of the structure function for electroproduction of π^0, (Ref. 17), to the sum of the structure functions for π^+ and π^- divided by 2.

variables p_T, $|\phi|$, and s. That range is 0.0 to 1.4 GeV/c in p_T, $\pi/3$ to π in $|\pi|$, and 15 to 31 GeV^2 in s. Furthermore, the correction for contribution from decay of exclusive ρ^0 is only included where explicitly stated.

A. Particle-type ratios

A major feature of this experiment and its predecessor is that the charge ratio for hydrogen $R^{\pm}$, defined as the cross section for positive hadrons over that for negative hadrons, increases dramatically as a function of Q^2 at high x_F. Furthermore, it can be seen in Fig. 6 that this increase as a function of Q^2 is a characteristic of the high x_F, or photon-fragmentation region. This increase at high x_F in the charge ratio as Q^2 increases is partly due to increased production of K^+ and p (see the K/π distributions in Ref. 13). Note that the data in Fig. 6 and Ref. 13 do not have the exclusive ρ^0 contribution subtracted, whereas the data in Ref. 2 do.

Integrating over x_F from 0.4 to 0.85, we can examine $R^{\pm}$ as a function of the other variables. Figures 7 and 8 show $R^{\pm}$ versus s and p_T for the same four bands in Q^2. No strong substructure in s is revealed, although there may be a systematic decline as s increases. However, Fig. 8 shows that at low Q^2, $R^{\pm}$ is definitely p_T dependent while at high Q^2 it is not. We know of no kinematic explanation for this; furthermore, the exclusive ρ^0 contribution does not produce this effect.

Figure 9 shows K^+/π^+, K^-/π^-, p/π^+, and $\bar{p}/\pi^-$ for both targets as a function of x_F. Here, the data have been integrated over Q^2 from 0.5 to 7.0 (GeV/c)^2 and a correction has been made for the exclusive ρ^0 contribution.

B. Invariant cross sections

1. ϕ dependence

Calculations within the context of the quark-parton model[14] show that variations as a function of

TABLE VII. $f(x_F)$ for all hadrons: four Q^2 ranges.

Q^2 [(GeV/c)^2]	x_F	Hydrogen h^-	Hydrogen h^+	Deuterium h^-	Deuterium h^+
0.42	0.05	0.294 ± 0.033	0.557 ± 0.070	0.312 ± 0.025	0.533 ± 0.049
0.42	0.15	0.163 ± 0.010	0.258 ± 0.015	0.170 ± 0.009	0.241 ± 0.013
0.42	0.25	0.113 ± 0.006	0.173 ± 0.009	0.117 ± 0.006	0.170 ± 0.009
0.42	0.35	0.082 ± 0.005	0.129 ± 0.007	0.086 ± 0.005	0.126 ± 0.007
0.42	0.45	0.061 ± 0.004	0.099 ± 0.006	0.067 ± 0.004	0.095 ± 0.005
0.42	0.55	0.048 ± 0.003	0.080 ± 0.005	0.053 ± 0.003	0.072 ± 0.004
0.42	0.72	0.035 ± 0.002	0.053 ± 0.003	0.040 ± 0.002	0.054 ± 0.003
0.42	0.92	0.018 ± 0.002	0.026 ± 0.002	0.021 ± 0.001	0.023 ± 0.002
0.72	0.05	0.274 ± 0.024	0.504 ± 0.048	0.297 ± 0.022	0.478 ± 0.034
0.72	0.15	0.179 ± 0.010	0.268 ± 0.014	0.180 ± 0.009	0.261 ± 0.014
0.72	0.25	0.115 ± 0.006	0.182 ± 0.010	0.124 ± 0.007	0.177 ± 0.009
0.72	0.35	0.079 ± 0.004	0.136 ± 0.007	0.085 ± 0.004	0.124 ± 0.006
0.72	0.45	0.059 ± 0.003	0.094 ± 0.005	0.065 ± 0.003	0.090 ± 0.005
0.55	0.55	0.047 ± 0.003	0.079 ± 0.004	0.048 ± 0.003	0.073 ± 0.004
0.72	0.72	0.030 ± 0.002	0.052 ± 0.003	0.034 ± 0.002	0.049 ± 0.003
0.72	0.92	0.017 ± 0.001	0.023 ± 0.002	0.016 ± 0.001	0.023 ± 0.001
1.4	0.05	0.202 ± 0.022	0.570 ± 0.062	0.270 ± 0.023	0.478 ± 0.040
1.4	0.15	0.190 ± 0.012	0.302 ± 0.017	0.190 ± 0.010	0.290 ± 0.016
1.4	0.25	0.110 ± 0.006	0.184 ± 0.010	0.118 ± 0.006	0.187 ± 0.010
1.4	0.35	0.077 ± 0.005	0.138 ± 0.008	0.083 ± 0.005	0.129 ± 0.007
1.4	0.45	0.053 ± 0.004	0.099 ± 0.006	0.057 ± 0.003	0.097 ± 0.005
1.4	0.55	0.038 ± 0.003	0.071 ± 0.005	0.040 ± 0.003	0.064 ± 0.004
1.4	0.72	0.022 ± 0.001	0.047 ± 0.003	0.026 ± 0.002	0.042 ± 0.002
1.4	0.92	0.012 ± 0.001	0.020 ± 0.002	0.013 ± 0.001	0.020 ± 0.001
3.1	0.05	0.449 ± 0.209	0.391 ± 0.079	0.246 ± 0.052	0.541 ± 0.143
3.1	0.15	0.200 ± 0.019	0.250 ± 0.018	0.186 ± 0.014	0.277 ± 0.019
3.1	0.25	0.097 ± 0.008	0.186 ± 0.013	0.118 ± 0.008	0.183 ± 0.011
3.1	0.35	0.078 ± 0.006	0.131 ± 0.009	0.073 ± 0.005	0.130 ± 0.008
3.1	0.45	0.040 ± 0.004	0.100 ± 0.008	0.051 ± 0.004	0.092 ± 0.006
3.1	0.55	0.032 ± 0.004	0.074 ± 0.007	0.036 ± 0.003	0.070 ± 0.005
3.1	0.72	0.015 ± 0.002	0.039 ± 0.003	0.017 ± 0.001	0.038 ± 0.003
3.1	0.92	0.009 ± 0.001	0.018 ± 0.002	0.010 ± 0.001	0.016 ± 0.002

ϕ in the electroproduction cross section might be expected. The best measurement to date, Ref. 15, found a small but not compelling variation for hydrogen.

Figure 10 shows the ϕ spectrum of the raw data at low Q^2. The large variation in this completely uncorrected data is caused by the 30-cm gap in the center of the appratus. This made it expressively difficult to measure the ϕ dependence with an accuracy superior to that of previous experiments. We can, however, measure quite well the ratio of production from deuterium to that from hydrogen as a function of ϕ, and Fig. 11 shows that result. Clearly, deuterium and hydrogen are quite similar with respect to hadron production in ϕ. No predictions have yet been made with which Fig. 11 can be compared.

As a check on the apparatus, we have measured the symmetry of the production of h^- in ϕ about ϕ equals 0; this result is shown in Fig. 12 for hydrogen and deuterium, separately.

2. p_T dependence

The invariant cross sections, averaged over $|\phi|$ from $\pi/3$ to π, are shown in Fig. 13 for $\langle Q^2 \rangle = 2.0$ (GeV/c)^2. Consistent with previous studies, we see an exponential drop as a function of $p_T{}^2$, the slope of which varies strongly as a function of x_F. This variation in $p_T{}^2$ and x_F is repeated over our entire Q^2 range from 0.35 to 7.0 (GeV/c)^2.

Although we do not present the other Q^2 bins in as much detail, Table IV and Fig. 14 show the average p_T for all x_F and Q^2 bins in the s range 15–31 GeV^2. First, the $\langle p_T \rangle$ values exhibit the well-known seagull effect[16] quite clearly. Hydrogen and deuterium results are the same to within the errors, which are largely statistical. At high x_F, $\langle p_T \rangle$ for positive hadrons is generally greater than that for negative hadrons. Also, at high x_F it can be seen that $\langle p_T \rangle$ increases as Q^2 increases. This latter effect is present in the pion-only data as well (see Table VI) and, according to our simula-

TABLE VIII. $f(x_F)$ for all pions: four Q^2 ranges.

Q^2 [(GeV/c)^2]	x_F	Hydrogen π^-	Hydrogen π^+	Deuterium π^-	Deuterium π^+
0.42	0.15	0.141 ± 0.014	0.206 ± 0.020	0.152 ± 0.013	0.185 ± 0.017
0.42	0.25	0.097 ± 0.007	0.128 ± 0.009	0.102 ± 0.006	0.137 ± 0.008
0.42	0.35	0.070 ± 0.005	0.093 ± 0.007	0.077 ± 0.005	0.097 ± 0.006
0.42	0.45	0.052 ± 0.004	0.064 ± 0.006	0.059 ± 0.004	0.071 ± 0.005
0.42	0.55	0.041 ± 0.004	0.059 ± 0.005	0.048 ± 0.003	0.056 ± 0.004
0.42	0.72	0.030 ± 0.002	0.043 ± 0.003	0.038 ± 0.002	0.046 ± 0.003
0.42	0.92	0.015 ± 0.002	0.021 ± 0.003	0.020 ± 0.002	0.021 ± 0.002
0.72	0.15	0.159 ± 0.014	0.228 ± 0.019	0.163 ± 0.012	0.208 ± 0.017
0.72	0.25	0.102 ± 0.006	0.147 ± 0.009	0.109 ± 0.006	0.142 ± 0.008
0.72	0.35	0.070 ± 0.005	0.103 ± 0.007	0.074 ± 0.004	0.094 ± 0.005
0.72	0.45	0.053 ± 0.004	0.068 ± 0.005	0.058 ± 0.003	0.067 ± 0.004
0.72	0.55	0.042 ± 0.003	0.059 ± 0.005	0.041 ± 0.003	0.054 ± 0.003
0.72	0.72	0.027 ± 0.002	0.040 ± 0.003	0.031 ± 0.002	0.036 ± 0.002
0.72	0.92	0.014 ± 0.001	0.021 ± 0.002	0.015 ± 0.001	0.019 ± 0.002
1.4	0.15	0.168 ± 0.017	0.249 ± 0.022	0.168 ± 0.014	0.232 ± 0.018
1.4	0.25	0.097 ± 0.007	0.141 ± 0.009	0.103 ± 0.006	0.152 ± 0.009
1.4	0.35	0.068 ± 0.005	0.101 ± 0.007	0.070 ± 0.005	0.091 ± 0.006
1.4	0.45	0.047 ± 0.004	0.072 ± 0.006	0.050 ± 0.003	0.069 ± 0.005
1.4	0.55	0.033 ± 0.003	0.051 ± 0.005	0.035 ± 0.003	0.045 ± 0.004
1.4	0.72	0.020 ± 0.002	0.034 ± 0.003	0.023 ± 0.002	0.030 ± 0.002
1.4	0.92	0.010 ± 0.001	0.016 ± 0.002	0.011 ± 0.001	0.016 ± 0.002
3.0	0.15	0.174 ± 0.021	0.179 ± 0.021	0.169 ± 0.018	0.219 ± 0.024
3.0	0.25	0.084 ± 0.009	0.132 ± 0.012	0.108 ± 0.009	0.138 ± 0.012
3.0	0.35	0.068 ± 0.006	0.093 ± 0.010	0.066 ± 0.006	0.094 ± 0.010
3.0	0.45	0.034 ± 0.005	0.075 ± 0.007	0.046 ± 0.005	0.066 ± 0.008
3.0	0.55	0.028 ± 0.004	0.055 ± 0.006	0.033 ± 0.004	0.051 ± 0.006
3.0	0.72	0.013 ± 0.002	0.029 ± 0.003	0.016 ± 0.002	0.029 ± 0.003
3.0	0.92	0.007 ± 0.003	0.014 ± 0.002	0.010 ± 0.001	0.012 ± 0.002

TABLE IX. $f(x_F)$ for pions, excluding contribution from exclusive ρ^0.

Q^2 [(GeV/c)^2]	x_F	Hydrogen π^- (excluding ρ^0)	Hydrogen π^+ (excluding ρ^0)	Deuterium π^- (excluding ρ^0)	Deuterium π^+ (excluding ρ^0)
0.42	0.15	0.140 ± 0.014	0.205 ± 0.020	0.151 ± 0.013	0.184 ± 0.017
0.42	0.25	0.094 ± 0.007	0.125 ± 0.009	0.099 ± 0.006	0.134 ± 0.008
0.42	0.35	0.065 ± 0.005	0.088 ± 0.007	0.073 ± 0.005	0.093 ± 0.006
0.42	0.45	0.045 ± 0.004	0.057 ± 0.006	0.053 ± 0.004	0.065 ± 0.005
0.42	0.55	0.032 ± 0.004	0.050 ± 0.005	0.040 ± 0.003	0.048 ± 0.004
0.42	0.72	0.018 ± 0.003	0.031 ± 0.003	0.028 ± 0.002	0.036 ± 0.003
0.42	0.92	0.009 ± 0.002	0.014 ± 0.003	0.014 ± 0.002	0.015 ± 0.002
0.72	0.15	0.157 ± 0.014	0.226 ± 0.019	0.161 ± 0.012	0.206 ± 0.017
0.72	0.25	0.100 ± 0.006	0.145 ± 0.009	0.107 ± 0.009	0.140 ± 0.008
0.72	0.35	0.066 ± 0.005	0.099 ± 0.007	0.071 ± 0.004	0.091 ± 0.005
0.72	0.45	0.048 ± 0.004	0.063 ± 0.005	0.053 ± 0.004	0.062 ± 0.004
0.72	0.55	0.035 ± 0.003	0.052 ± 0.005	0.034 ± 0.003	0.048 ± 0.003
0.72	0.72	0.018 ± 0.002	0.031 ± 0.003	0.022 ± 0.002	0.027 ± 0.002
0.72	0.92	0.010 ± 0.002	0.016 ± 0.002	0.010 ± 0.002	0.014 ± 0.002
1.4	0.15	0.166 ± 0.017	0.247 ± 0.022	0.166 ± 0.014	0.230 ± 0.018
1.4	0.25	0.095 ± 0.007	0.139 ± 0.009	0.101 ± 0.006	0.150 ± 0.009
1.4	0.35	0.065 ± 0.005	0.098 ± 0.007	0.068 ± 0.005	0.089 ± 0.006
1.4	0.45	0.043 ± 0.004	0.068 ± 0.006	0.046 ± 0.004	0.066 ± 0.005
1.4	0.55	0.028 ± 0.003	0.046 ± 0.005	0.030 ± 0.003	0.040 ± 0.004
1.4	0.72	0.013 ± 0.002	0.028 ± 0.003	0.017 ± 0.002	0.024 ± 0.002
1.4	0.92	0.007 ± 0.002	0.012 ± 0.002	0.008 ± 0.001	0.013 ± 0.002
3.0	0.15	0.173 ± 0.021	0.178 ± 0.021	0.168 ± 0.018	0.218 ± 0.024
3.0	0.25	0.082 ± 0.009	0.130 ± 0.012	0.106 ± 0.009	0.136 ± 0.012
3.0	0.35	0.066 ± 0.006	0.091 ± 0.010	0.065 ± 0.006	0.093 ± 0.010
3.0	0.45	0.032 ± 0.005	0.073 ± 0.007	0.044 ± 0.005	0.064 ± 0.008
3.0	0.55	0.025 ± 0.004	0.052 ± 0.006	0.030 ± 0.004	0.048 ± 0.006
3.0	0.72	0.010 ± 0.002	0.026 ± 0.003	0.013 ± 0.002	0.026 ± 0.003
3.0	0.92	0.006 ± 0.003	0.013 ± 0.002	0.008 ± 0.002	0.011 ± 0.002

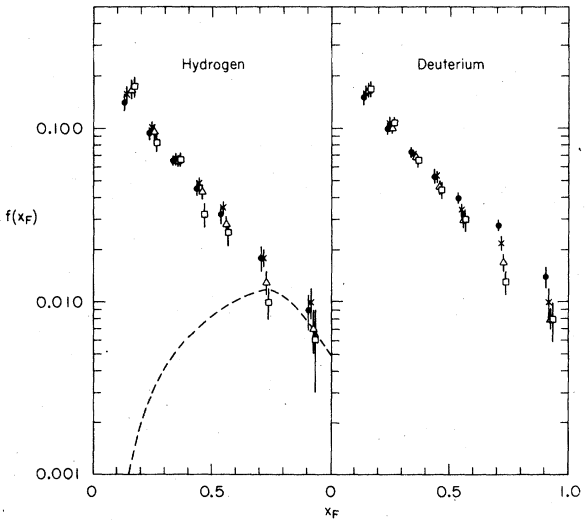

FIG. 19. Comparison of the structure function for π^- for four Q^2 bands, excluding the ρ^0 contribution. The symbols are as shown in Fig. 6. The dashed line is the estimated exclusive ρ^0 contribution for the lowest Q^2 band.

tion studies, is not due to the contribution from decay of exclusively produced ρ^0.

Figure 15 and Table V show the average p_T for all s and Q^2 bands for the data after integrating

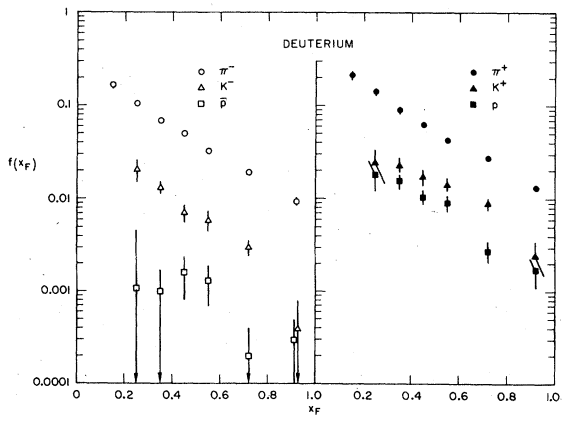

FIG. 20. $f(x_F)$ for deuterium for the kinematic range 0.5 to 7.0 (GeV/c)^2 in Q^2. The data appear also in Table X.

TABLE X. $f(x_F)$ and particle-type ratios for the kinematic range 0.5 to 7.0 $(\mathrm{GeV}/c)^2$ in Q^2; $\langle Q^2\rangle = 1.2$ $(\mathrm{GeV}/c)^2$.

x_F	π	p	K	p/π	K/π
			negatives, hydrogen		
0.15	0.163 ± 0.010	...	...	...	...
0.25	0.098 ± 0.006	0.0072 ± 0.0067	0.0056 ± 0.0093	0.073 ± 0.068	0.057 ± 0.095
0.35	0.063 ± 0.004	0.0029 ± 0.0014	0.0115 ± 0.0030	0.046 ± 0.023	0.183 ± 0.051
0.45	0.043 ± 0.003	0.0019 ± 0.0010	0.0069 ± 0.0021	0.044 ± 0.022	0.161 ± 0.053
0.55	0.032 ± 0.002	0.0012 ± 0.0008	0.0033 ± 0.0016	0.038 ± 0.024	0.101 ± 0.052
0.72	0.016 ± 0.001	0.0002 ± 0.0002	0.0020 ± 0.0006	0.013 ± 0.014	0.122 ± 0.041
0.92	0.009 ± 0.001	0.0003 ± 0.0004	0.0004 ± 0.0010	0.033 ± 0.044	0.043 ± 0.112
			positives, hydrogen		
0.15	0.228 ± 0.013	...	...	...	...
0.25	0.139 ± 0.008	0.0296 ± 0.0111	0.0149 ± 0.0156	0.212 ± 0.080	0.107 ± 0.112
0.35	0.099 ± 0.006	0.0146 ± 0.0032	0.0246 ± 0.0054	0.148 ± 0.033	0.250 ± 0.059
0.45	0.066 ± 0.004	0.0130 ± 0.0024	0.0148 ± 0.0042	0.197 ± 0.036	0.224 ± 0.070
0.55	0.050 ± 0.004	0.0073 ± 0.0019	0.0138 ± 0.0035	0.144 ± 0.039	0.274 ± 0.079
0.72	0.027 ± 0.002	0.0041 ± 0.0010	0.0110 ± 0.0019	0.150 ± 0.036	0.402 ± 0.080
0.92	0.014 ± 0.001	0.0006 ± 0.0006	0.0031 ± 0.0011	0.043 ± 0.043	0.219 ± 0.088
			negatives, deuterium		
0.15	0.165 ± 0.009	...	...	...	...
0.25	0.105 ± 0.006	0.0017 ± 0.0017	0.0207 ± 0.0052	0.016 ± 0.016	0.198 ± 0.051
0.35	0.068 ± 0.004	0.0010 ± 0.0007	0.0132 ± 0.0018	0.015 ± 0.011	0.194 ± 0.029
0.45	0.050 ± 0.003	0.0016 ± 0.0008	0.0071 ± 0.0015	0.032 ± 0.015	0.144 ± 0.033
0.55	0.032 ± 0.002	0.0013 ± 0.0006	0.0059 ± 0.0014	0.042 ± 0.020	0.187 ± 0.047
0.72	0.019 ± 0.001	0.0002 ± 0.0002	0.0030 ± 0.0005	0.009 ± 0.008	0.158 ± 0.031
0.92	0.009 ± 0.001	0.0003 ± 0.0002	0.0004 ± 0.0004	0.029 ± 0.024	0.046 ± 0.046
			positives, deuterium		
0.15	0.214 ± 0.012	...	...	...	...
0.25	0.143 ± 0.008	0.0183 ± 0.0067	0.0245 ± 0.0096	0.129 ± 0.047	0.172 ± 0.068
0.35	0.090 ± 0.005	0.0154 ± 0.0026	0.0228 ± 0.0041	0.171 ± 0.029	0.254 ± 0.049
0.45	0.063 ± 0.004	0.0106 ± 0.0017	0.0172 ± 0.0029	0.168 ± 0.027	0.272 ± 0.050
0.55	0.043 ± 0.003	0.0090 ± 0.0017	0.0141 ± 0.0026	0.212 ± 0.039	0.331 ± 0.068
0.72	0.027 ± 0.002	0.0027 ± 0.0006	0.0087 ± 0.0011	0.098 ± 0.022	0.317 ± 0.047
0.92	0.013 ± 0.001	0.0017 ± 0.0006	0.0025 ± 0.0010	0.129 ± 0.044	0.190 ± 0.084

over x_F from 0.4 to 0.85. Both charge signs and both targets have the same behavior: $\langle p_T\rangle$ increases steadily as s increases. Furthermore, this increase may be somewhat more steep at high Q^2 than at low Q^2.

Figure 16 shows the invariant cross sections for all hadrons (h^+,h^-), pions only $(\pi^+,\ \pi^-)$, kaons only (K^+,K^-), and protons (p). The kinematic range covered is $15<s<31$ GeV^2 and $0.4<x_F<0.85$. "Low Q^2" refers to 0.35 to 1.0 $(\mathrm{GeV}/c)^2$, and "High Q^2" refers to 1.0 to 7.0 $(\mathrm{GeV}/c)^2$. The straight lines are least-squares fits to the form $e^{-bp_T^2}$; Table VI shows the resulting value of b for each particle type. Owing to lack of statistics, K^- is omitted from the fits and $\bar{p}$ is omitted from the figure. Note that K^+ has a consistently smaller value of b than π^+. Also, values of b for low Q^2 are significantly larger than those for high Q^2. This fact is reflected in Figs. 14 and 15 and is consistent with the findings in Ref. 1.

3. x_F dependence

When the invariant cross section is integrated over $p_T{}^2$, one is left with the structure function $f(x_F)$. In Fig. 17 we compare our result for $f(x_F)$ to that of a μp streamer-chamber experiment.[15] Extracting $f(x_F)$ for π^+ and π^- and summing and dividing by 2, we can compare Fig. 18 to data from Berger *et al.*[17] Note that Ref. 17 employs the variable z defined as p_{lab}/ν.

Table VII presents $f(x_F)$ for all hadrons for the four Q^2 bands. It is of interest that the dropoff as a function of x_F becomes steeper as Q^2 increases, especially for h^-. This trend is repeated in $f(x_F)$ for pions (Table VIII). The only other experiment

TABLE XI. $f(x_F)$ and particle-type ratios averaged over the range 0.4 to 0.85 in x_F and excluding the ρ^0 contribution.

Q^2 [(GeV/c)^2]	Hydrogen		Deuterium	
	π^-	π^+	π^-	π^+
0.42	0.0304 ± 0.0016	0.0416 ± 0.0022	0.0373 ± 0.0010	0.0464 ± 0.0014
0.72	0.0293 ± 0.0012	0.0436 ± 0.0023	0.0327 ± 0.0007	0.0414 ± 0.0010
1.4	0.0252 ± 0.0012	0.0407 ± 0.0022	0.0273 ± 0.0009	0.0384 ± 0.0013
3.0	0.0188 ± 0.0021	0.0418 ± 0.0045	0.0234 ± 0.0018	0.0402 ± 0.0031
	K^-/π^-	K^+/π^+	K^-/π^-	K^+/π^+
0.42	0.18 ± 0.05	0.40 ± 0.08	0.12 ± 0.02	0.21 ± 0.04
0.72	0.15 ± 0.04	0.32 ± 0.05	0.16 ± 0.02	0.30 ± 0.04
1.4	0.06 ± 0.05	0.26 ± 0.09	0.15 ± 0.04	0.35 ± 0.06
3.0	0.22 ± 0.18	0.22 ± 0.17	0.19 ± 0.12	0.10 ± 0.13
	$\bar{p}/\pi^-$	p/π^+	$\bar{p}/\pi^-$	p/π^+
0.42	0.01 ± 0.01	0.14 ± 0.03	0.01 ± 0.01	0.12 ± 0.02
0.72	0.02 ± 0.01	0.13 ± 0.03	0.02 ± 0.01	0.14 ± 0.02
1.4	0.06 ± 0.03	0.24 ± 0.05	0.04 ± 0.02	0.15 ± 0.03
3.0	0.00 ± 0.11	0.20 ± 0.09	0.00 ± 0.07	0.29 ± 0.08

reporting a similar effect is Bebek *et al.*[18] However, when the estimated contribution from ρ^0 is subtracted from our data, as in Table IX and Fig. 19, this effect practically disappears in the π^+ and is much lessened in the π^- results. Since the analysis in Ref. 18 does not address this question, it is not clear how much of the effect reported there might be due to the decay products from the exclusive ρ^0 final state or from other processes available at lower s.

Figure 20 and Table X show $f(x_F)$ for π^+, π^-, K^+, K^-, p, and $\bar{p}$ with the contribution from ρ^0 subtracted. The kinematic range is from 0.5 to 7.0 (GeV/c)^2 in Q^2, with $\langle Q^2\rangle = 1.2$ (GeV/c)^2. The two rightmost columns of Table X show the K/π and p/π ratios as a function of x_F.

4. Q^2 dependence

Table XI shows the structure functions for hadrons and pions after averaging over x_F from 0.4 to 0.85. The contribution from exclusive ρ^0 has been subtracted. Notice that π^+ and h^+ show very little dependence on Q^2, whereas π^- and h^- decrease significantly.

ACKNOWLEDGMENTS

We wish to acknowledge the important support and enthusiasm contributed by numerous groups at SLAC, in particular, the technical staff of Group E: R. Baggs, R. Leonard, A. Newton, R. Stickley, and M. Stoddard. Fred Martin was invaluable in the early stages of the experiment, contributing especially to the design and operation of the superconducting tube. We are indebted to A. Seiden and T. Schalk for numerous discussions and comparisons with their data. Finally, we thank the SLAC theory group for the interest they have displayed. This work was supported by the U. S. Department of Energy.

*Present address: Department of Physics, University of California, La Jolla, California 92037.
†Present address: Lawrence Berkeley Laboratory, University of California, Berkeley, California 94320.
‡Present address: Bell Laboratories, Murray Hill, New Jersey 07974.
§Present address: General Electric Research and Development, Schenectady, New York 12301.

[1]J. T. Dakin *et al.*, Phys. Rev. D 10, 1401 (1974); J. T. Dakin and G. J. Feldman, *ibid.* 2862 (1973).
[2]J. F. Martin *et al.*, Phys. Lett. 65B, 483 (1976).
[3]J. F. Martin and L. S. Osborne, Phys. Rev. Lett. 38, 1193 (1977).
[4]L. S. Osborne *et al.*, Phys. Rev. Lett. 40, 1624 (1978).
[5]W. L. Lakin *et al.*, Nucl. Instrum. Methods 103, 431 (1972).
[6]W. L. Lakin and R. E. Baggs, Nucl. Instrum. Methods 102, 367 (1972).
[7]D. Yount, Nucl. Instrum. Methods 52, 1 (1967).
[8]D. G. Roth, M. I. T. Ph.D. thesis, 1976 (unpublished).
[9]W. B. Atwood and G. B. West, Phys. Rev. D 7, 773 (1973).

[10]S. Stein *et al.*, Phys. Rev. D 12, 1884 (1975).
[11]A. Bodek *et al.*, Phys. Lett. 51B, 417 (1974).
[12]W. B. Atwood, SLAC Report No. SLAC-185 (unpublished); W. B. Atwood *et al.*, Phys. Lett. 64B, 479 (1976).
[13]J. F. Martin *et al.*, Phys. Rev. Lett. 40, 283 (1978).
[14]H. Georgi and H. D. Politzer, Phys. Rev. Lett. 40, 3 (1978); F. Ravndal, Phys. Lett. 43B, 301 (1973).
[15]C. del Papa *et al.*, Phys. Rev. D 15, 2425 (1977).
[16]L. Hand, in *Proceedings of the International Symposium on Lepton and Photon Interactions at High Energies, Hamburg, 1977*, edited by F. Gutbrod (DESY, Hamburg, 1977).
[17]Ch. Berger *et al.*, Phys. Lett. 70B, 471 (1977) and an unpublished paper.
[18]C. J. Bebek *et al.*, Phys. Rev. Lett. 37, 1525 (1976).